# Emission Characterization of Porous Electrospray Thrusters with Actively Controlled Flow Rate

**IEPC-2022-191**

*Presented at the 37th International Electric Propulsion Conference*
*Massachusetts Institute of Technology, Cambridge, MA, USA*
*June 19-23, 2022*

Chengyu Ma[1], Vincenzo Messina[2], and Charles N. Ryan[3]
*University of Southampton, Southampton, Hampshire, United Kingdom, SO17 1BJ*

Joshua L. Rovey[4], Zachary R. Putnam[5], and Michael Lembeck[6]
*University of Illinois Urbana-Champaign, Urbana, IL 61801, United States*

Steven Berg[7]
*Froberg Aerospace LLC., Wilmington, NC 28401, United States*

**A pressurized propellant feeding system was designed and tested for a porous-emitter electrospray thruster. The system provides a preliminary design for an electrospray-monopropellant dual-mode propulsion system that uses a HAN-based ionic liquid propellant. For ease of initial experimental validation, a conventional ionic liquid propellant, EMI-$BF_4$, was used in this pressurize-feeding electrospray system. The dry thruster was fed from a pressurized propellant storage beaker via a tubing. The dimensions of the feeding tube were calculated to deliver the nominal flow rate. In order to reduce the time of filling the thruster, a bypass feeding line with a high flow rate was integrated into the system. The transient behavior of the fluidic impedance and flow rate during the initial propellant filling stage were computed for analysis. The flow rates and propellant feeding performance using both the nominal and bypass feeding lines were tested and proved effective. The current-voltage characteristics of the electrospray thruster were measured in vacuum tests, with the propellant delivery pressure changed from 1 bar to 0 bar. The current values at the negative polarity significantly increased with higher feeding pressure, whilst the positive currents only experienced minor variations. With the pressure changing from 1 bar to 0 bar, the current at -3000 V changed from -807.54 $\mu$A to -217.18 $\mu$A, whilst in comparison, the current at +3000 V only varied from +216.52 $\mu$A to +300.29 $\mu$A. This preliminary design and test demonstrated that using a pressurized propellant feeding system on an electrospray thruster with a porous emitter is feasible. This opens up the possibility that the electrospray emission performance can be controlled not only by the thruster voltage but also by the propellant delivery pressure.**

## I. Nomenclature

$\Delta P$ = pressure difference for feeding the propellant
$Z$ = fluidic impedance

[1]Research Fellow, Department of Aeronautics and Astronautics, Southampton, Hampshire, SO17 1BJ, United Kingdom.
[2]Graduate Research Assistant, Department of Aeronautics and Astronautics, Southampton, Hampshire, SO17 1BJ, United Kingdom.
[3]Lecturer/Assistant Professor, Department of Aeronautics and Astronautics, Southampton, Hampshire, SO17 1BJ, United Kingdom.
[4]Associate Professor, Aerospace Engineering, Talbot Laboratory 104 S Wright St, Urbana, IL 61801, United States.
[5]Assistant Professor, Aerospace Engineering, Talbot Laboratory 104 S Wright St, Urbana, IL 61801, United States.
[6]Clinical Associate Professor, Aerospace Engineering, Talbot Laboratory 104 S Wright St, Urbana, IL 61801, United States.
[7]Assistant Professor, Chief Executive Office, Froberg Aerospace LLC, 226 N. Front St. Ste. 123, Wilmington, NC 28401, United States.

$R$ = capillary inner radius
$\mu$ = liquid dynamic viscosity
$\kappa$ = permeability of the porous material
$A_p$ = cross-section area of the porous material relative to the flow direction
$\epsilon$ = porosity of the porous bed
$D_p$ = average diameter of packed solids
$\Phi_s$ = sphericity of the particles in the packed bed
$\gamma$ = liquid surface tension
$R_x$, $R_y$ = principle radii of the liquid-vacuum boundary curvature
$P_{ext}$ = pressure created on emitter tips from electrospray emission

## II. Introduction

Electrospray propulsion is an electrostatic propulsion concept that uses a strong static electric field to extract and accelerate charged particles from a liquid propellant. Over the development of the last two decades, it has demonstrated competitive performance in specific impulse and efficiency and is now viewed as a promising micro-propulsion option in a wide range of nanosatellite applications [1]. A primary type of electrospray thruster now under development uses a porous emitter coupled to a porous reservoir, in which the propellant is fed to the emitter passively using capillary actions. In a passively-fed electrospray configuration, the effects of Laplace pressure difference between the liquid-vacuum interfaces in the porous emitter and the porous reservoir have been studied [2]. The Laplace pressures at the two sides would eventually reach a balanced and static state before electrospray emission. During electrospray emission, the electrostatic extraction of liquid propellant at emitter tips would introduce a loss of pressure, breaching this pre-balanced state and creating a Laplace pressure difference between the emitter and the reservoir. The newly generated pressure difference pushes the propellant towards the emission tips and automatically sustains the electrospray process. This configuration eliminates the need for a pressurized propellant delivery system, and the propulsion system size can be made more compact. Passively-fed electrospray thrusters have demonstrated mixed ion-droplet and purely ionic emission, capable of delivering high specific impulse from 1000 to 4000 s [3–6]. However, the thrust generated from ionic-emission electrospray thrusters is generally limited to less than 200 $\mu$N. The low thrust constrains the potential applications of electrospray thrusters, limiting their potential use to high change-in-velocity missions for nanosatellites, or precision control of satellites. Currently, ionic-emission electrospray thrusters are only suited for high velocity-change nanosatellite missions with slow accelerations.

In order to expand the applicable mission scenarios using electrospray thrusters, multimode propulsion systems that consist of a high-thrust monopropellant chemical thruster and a high-specific-impulse electrospray thruster are being developed worldwide [7–9]. The two thrusters would use the same propellant, with the monopropellant decomposition chemical thruster providing high thrust and the electrospray thruster providing high specific impulse. Different propellants are being developed for this concept, mostly hydroxylammonium nitrate (HAN) based propellants, such as ASCENT, GEM [9] and FAM-110A [8]. Here we aim to investigate the HAN-based FAM-110A propellant, a novel ionic liquid developed by the University of Illinois Urbana-Champaign consisting of 59% of HAN and 41% of 1-Ethyl-3-methylimidazolium ethyl sulfate (EMIM-Et$SO_4$) [8]. The propellant is to be delivered to the chemical thruster and the electrospray thruster from the same storage tank using a pressurized propellant delivery method, as illustrated in Figure 1. With the same propellant being able to be quickly switched between the chemical and electric modes, this system would offer highly flexible maneuverability to suit complicated and variable mission requirements. FAM-110A propellant has been tested in a capillary-emitter electrospray thruster, and verified the compatibility of using FAM-110A for electrospray emission [8, 10, 11]. Here we aim to validate FAM-110A's performance in a porous-emitter type electrospray thruster using the PET-100 electrospray thruster developed at the University of Southampton, which has demonstrated high emission current output [6, 12].

Note that the pressure-feeding electrospray thruster system potentially has advantages as a stand-alone propulsion system even without integrating the high-thrust chemical mode thruster. An electrospray thruster using a passive propellant feeding method has a limitation in the total amount of propellant it can carry, constrained by the size of the porous reservoir. The overall deliverable impulse is considerably limited unless using a sizeable porous reservoir, which in turn significantly increases the dry mass. The design here would overcome this limitation in total impulse by pressure-feeding the propellant from a large-volume propellant storage tank. Another advantage of the pressure-feeding propellant delivery system is its more tunable electrospray performance. In conventional passively-fed electrospray thrusters, the propulsive performance in thrust and specific impulse is only throttleable within a small range, since

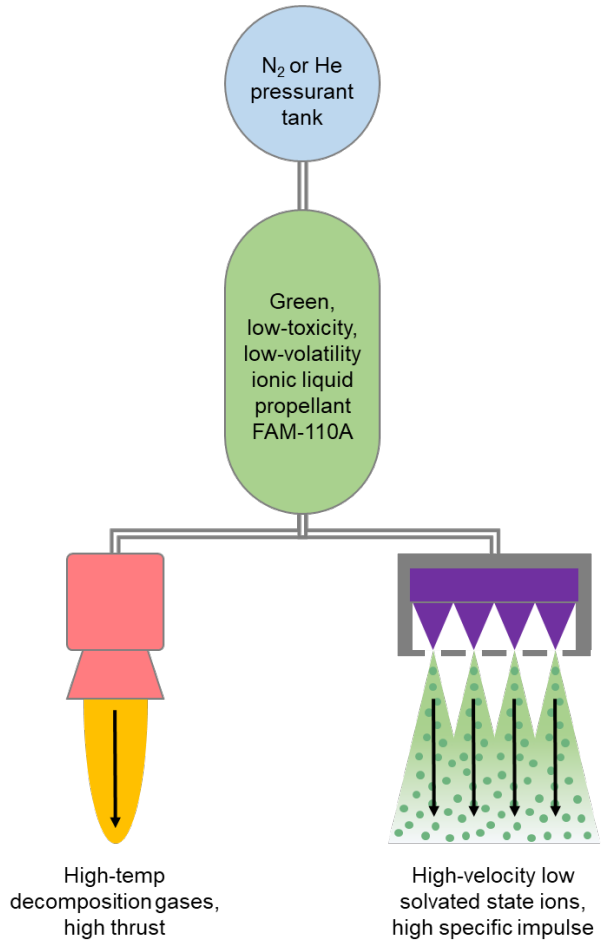


**Fig. 1 The decomposition-electrospray multimode propulsion concept using FAM-110A ionic liquid propellant [7].**

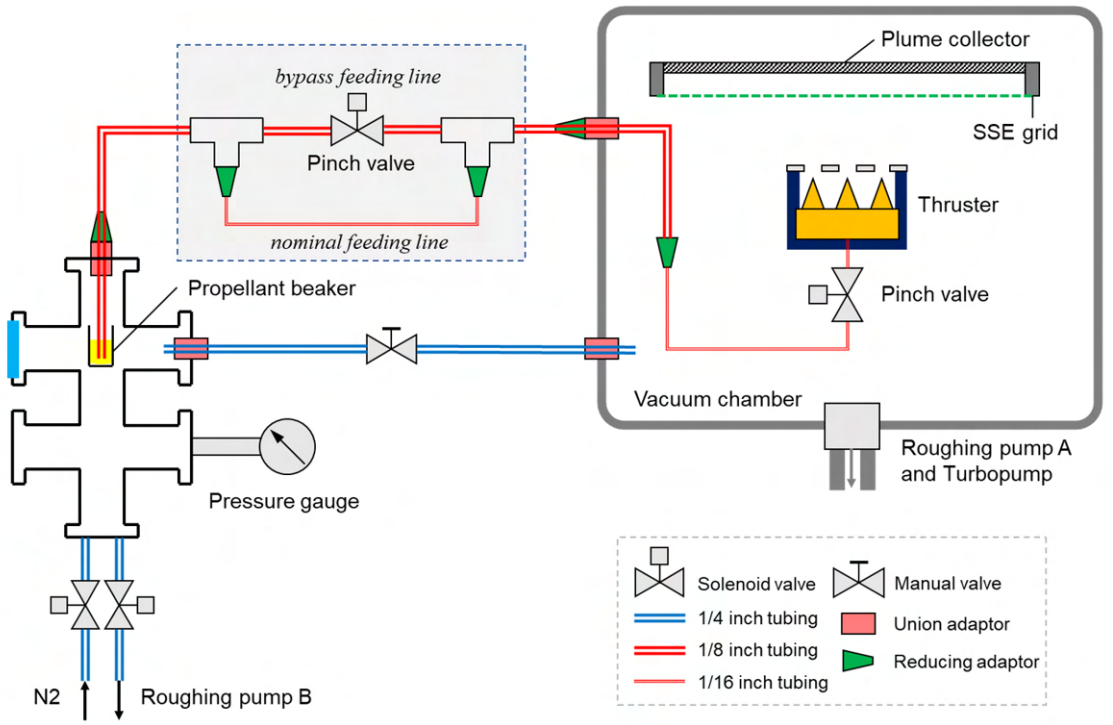


**Fig. 2 Pressurized propellant feeding system concept in the laboratory testing.**

the voltage between the emitter and the extractor is the sole performance control factor in a passively-fed porous emitter electrospray thruster. In electrospray thrusters using capillary type emitters, the propellant flow rate can be controlled using a pressurized propellant delivery system, which can result in different electrospray onset voltages, current-voltage characteristics, emission stability, and plume particle compositions. The effects of flow rate on capillary electrospray emitter performance have been investigated in multiple studies [13–16]. As a well-known example, the Colloid Milli-Newton Thruster (CMNT) with capillary electrospray emitters developed for the Laser Interferometer Space Antenna (LISA) Pathfinder mission was coupled with a pressurized propellant delivery system [17]. However, as porous electrospray emitters usually rely on capillary actions to spontaneously supply propellant, research on actively feeding a porous-emitter electrospray thruster is currently highly scarce [18], and the effects of actively controlled flow rates on electrospray performance are not well understood.

This study aims to investigate the electrospray performance and plume properties using an active pressurized delivery system with FAM-110A propellant. However, as FAM-110A propellant contains the highly toxic and carcinogenic composition HAN and has an inherent tendency for rapid decomposition, a less toxic and widely used ionic liquid, 1-ethyl-3-methylimidazolium tetrafluoroborate (EMI-$BF_4$), was tested first to verify the propellant delivery system design. This paper only discusses the preliminary results of pressurized electrospray using EMI-$BF_4$, from which the propellant pressure-delivery system will be improved in the following iteration to test the performance of FAM-110A propellant.

## III. Propellant Delivery System Design

As a preliminary design for laboratory investigation, the propellant delivery system consists of two major sections, as illustrated in Figure 2. The section inside the vacuum chamber includes the main electrospray thruster, a valve, and the propellant delivery tubing connecting the thruster to a fluidic feedthrough on a vacuum chamber flange. The section outside the vacuum chamber includes a small 6-way cross vacuum enclosure, a vacuum pump, and a flow rate restriction tubing system.

The EMI-$BF_4$ propellant is placed in a beaker in the 6-way cross vacuum enclosure of KF40 flanges, and the propellant feeding tubing end is placed inside the beaker near the bottom. During thruster operation, the main test chamber where the thruster is placed is in vacuum, and pressure in the small 6-way vacuum enclosure is controlled from

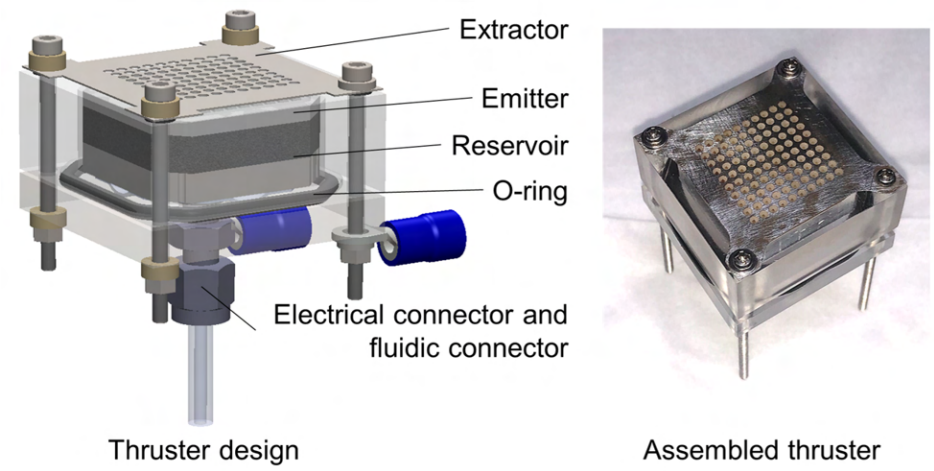


**Fig. 3 Modified PET-100 thruster for pressurized propellant feeding.**

1 bar to near vacuum using a nitrogen tank. An electrical pressure sensor with analogue output sourced from Honeywell International Inc. was mounted on the a flange of the 6-way enclosure, and the pressure signal was collected using an National Instruments analogue input card. Using a pulse-mode feedback loop control method based on the pressure sensor reading, the pressure in the 6-way cross was varied from $10^{-2}$ mbar to 1 bar by controlling solenoid valves to the nitrogen tank and the roughing pump.

The thruster used in this study is a slightly modified PET-100 thruster, as shown in Figure 3 [19, 20]. The thruster uses an emitter chip CNC machined from P5 grade porous borosilicate glass. The emitter has a $10 \times 10$ array of emission tips, whose average emitter height is 1.88 mm with a standard deviation of 7.5 $\mu$m, and the average emission tip radius is 45.1 $\mu$m with a standard deviation of 7.4 $\mu$m. A P0 grad porous glass reservoir was placed underneath the emitter. The reservoir had larger pore sizes than that of the emitter, making it possible for the thruster to work in a passive-fed mode from capillary actions. The 0.2 mm thick extractor sheet had 100 apertures with the diameter of 1.5 mm, and the apertures were aligned with the emission tips. Note that due to schedule reasons, the extractor in this EMI-$BF_4$ study was made of mild steel, not ideal materials of titanium (with high chemical resistance to FAM-110A propellant) or molybdenum (with low sputter yield). A Swagelok 1/16 inch bulkhead union made of 316 stainless steel is connected to the thruster backside, working as an electrical connector to the power supply as well as a fluidic connector for the propellant feeding tubing. In order to avoid contamination between EMI-$BF_4$ and FAM-110A liquids, two copies of the same thruster and emitter were manufactured, one for each propellant.

High voltages are to be applied in the thruster, with the extractor being ground potential, and the emitter and reservoir having high potential to the ground. As the ionic liquid propellant is electrically conductive, the entire propellant feeding line and the liquid storage beaker in the 6-way cross will have high potential. Proper electrical insulation designs need to be applied to avoid electrical breakdown or shorting between the propellant delivery system and grounded testing facilities. The propellant delivery tubing is made of fluorinated ethylene propylene (FEP) material, which has good chemical resistance, a promising material to be used with reactive HAN-based FAM-110A propellant. The beaker in the 6-way cross was placed on a cylindrical acrylic block. The Swagelok compression-type fluidic feedthroughs on the vacuum flanges are bored through, where the FEP tubing goes through the bore connectors, keeping the system leak-tight.

## IV. Propellant Flow Rate Design

The required flow rate of EMI-$BF_4$ propellant to be delivered to the PET-100 thruster was estimated from previous plume composition work using a time-of-flight (ToF) system, which is approximately from 1 to 10 $\mu$g/s, under the assumption of a purely ionic emission mode [6]. With the EMI-$BF_4$ ionic liquid density of 1.294 g/cm$^3$ at 25 °C room temperature, the required volumetric flow rate ranges from $7.73 \times 10^{-4}$ mm$^3$/s to $7.73 \times 10^{-3}$ mm$^3$/s.

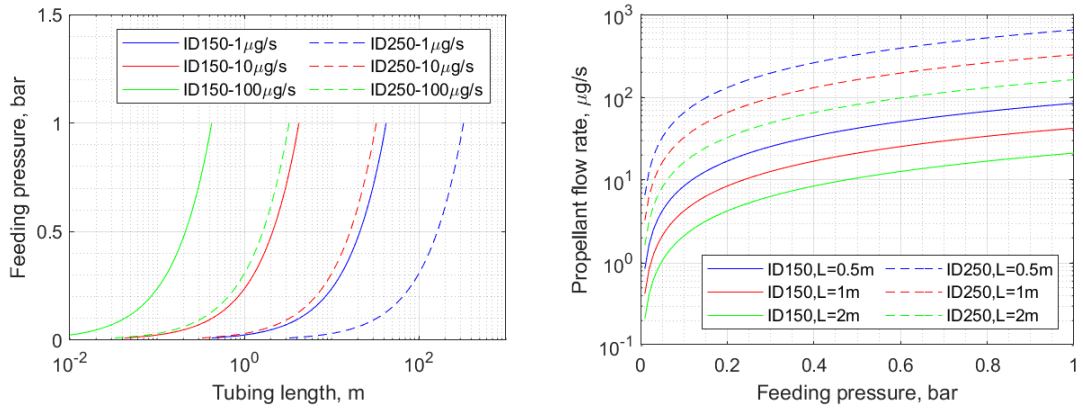


(a) Tubing length and required feeding pressure for 1, 10 and 100 $\mu$g/s flow rate. Tubing inner diameters are 150 and 250 $\mu$m.

(b) Flow rate at different feeding pressures with fixed tubing length of 0.5, 1 and 2 m. Tubing inner diameters are 150 and 250 $\mu$m.

**Fig. 4 The effect of tubing inner diameter, tubing length and feeding pressure on the nominal propellant flow rate.**

### A. Nominal flow tubing

In the initial investigation, the propellant delivery method used one long, thin tubing to limit the flow rate, with the designed tubing to be used as a core component in the nominal propellant feeding line. The propellant flow is pressure-driven flow inside a cylindrical capillary, the volumetric flow rate, $Q$, can be estimated using Poiseuille's Law, which in standard fluidic-kinetic notation is described as

$$Q = \frac{\Delta P}{Z} = \frac{\Delta P \pi R^4}{8 \mu L}, \tag{1}$$

where $\Delta P$ is the pressure difference between the front side and the back side, $Z$ is the equivalent fluidic impedance, $R$ is the capillary inner radius, $\mu$ is the dynamic viscosity of the liquid, and $L$ is the length of the capillary.

The dynamic viscosity of EMI-$BF_4$ at room temperature is approximately 0.038 Pa·s. Thinner tubing can reduce the flow rate effectively, but it is more prone to getting clogged by impurity particles without a filter placed in the upstream of the flow. Therefore, FEP tubing components with the inner diameter of 150 $\mu$m and 250 $\mu$m were selected for study. Based on the Equation 1, the relationships among propellant flow rate, propellant feeding pressure, tubing length and tubing inner diameter are illustrated in Figure 4 The results suggest that tubing (150 $\mu$m or 250 $\mu$m) with a length of 1.1 m and 2.1 m should cover the whole flow rate range expected in a PET-100 electrospray thruster.

### B. Flow Resistance Management

Initially, the porous materials in the thruster were already soaked with ionic liquid propellant before the pressurized propellant testing. However, two significant drawback were found in this propellant feeding method. As the pre-soaked thruster feeding tube is to be inserted in the propellant storage beaker, it was highly probable that some air bubbles get entrapped in the tubing between the thruster and the propellant beaker. As the pressure was decreased for vacuum testing, the entrapped air bubbles would expand significantly, pushing liquid flowing toward the vacuum side, likely causing propellant flooding or forming popping bubbles that induce short circuits. The severity of this problem can be somewhat mitigated by pre-vacuuming the propellant and the 6-way cross chamber, to reduce the amount of absorbed water vapor and guide the outgasing to the reversed direction, respectively. With careful preparation and operation of such procedures, it was possible that the air bubbles would not cause thruster to fail. However, another issue was found with this feeding method. As the porous emitter was pre-soaked with propellant, the thruster could start electrospray emission even without pressure from the back, functioning as a conventional passive-fed electrospray thruster. Thus it was difficult to identify when or whether the pressurized propellant feeding starts to affect the thruster performance. The time at which the external pressure starts to act can be roughly estimated using flow rate calculation, but experimental confirmation of this starting time proved to be difficult.

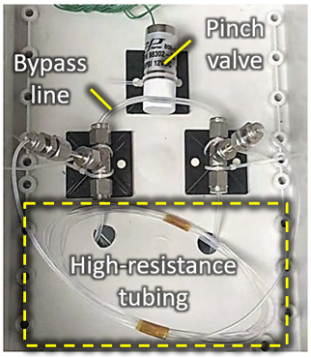


**Fig. 5 The flow resistance management system.**

In order to solve the problems with entrapped air bubbles and determine the start time of pressurized propellant feeding, a different pre-test preparation approach was investigated in this study. The emitter, reservoir, and propellant feeding tubes were thoroughly dried before the test. Note that due to the low vapor pressure of EMI-$BF_4$, drying the porous materials after being soaked with ionic liquid was more difficult. The porous materials containing EMI-$BF_4$ were repeatedly rinsed in a 50 ml beaker using isopropanol alcohol (IPA). After about ten times, the emitter and the reservoir were placed in an ultrasonic cleaner using IPA solution for 30 minutes at room temperature. The final stage of drying porous substrates was using a hot air gun. After these steps, the porous materials were visually inspected and tested using a multimeter. If the electrical resistance measurement between the front and back surfaces showed 'open line', the materials were deemed sufficiently dried and ready to be reused. The P5 grade emitter has smaller pore sizes than the P0 grade reservoir, so it took more attempts to dry. The propellant in the beaker was also thoroughly outgassed in a vacuum before being used for thruster testing. The whole test system was assembled after these preparations. The gate valve between the 6-way cross chamber and the thruster test chamber was open, and vacuuming was started at both chambers, keeping their pressures balanced. As the emitter and the reservoir were dry, the air pressure inside the tubing would be nearly the same as the vacuum chamber pressure. When the chambers reached a high vacuum at the level of $10^{-5}$ mbar, the manual valve connecting the 6-way cross chamber and the thruster test chamber was closed, and the pressure in the 6-way cross chamber could be increased up to 1 bar, pushing the propellant from the beaker toward to thruster. The thruster would be filled with the EMI-$BF_4$, with little to no air bubbles. In order to avoid propellant overflowing during the propellant-filling, a high voltage was kept between the emitter and the extractor. Electrospray emission would start once the propellant was sufficiently filled up in the thruster. A triggering signal from LabVIEW was then sent to turn off the pinch valve in the propellant feeding line and stop the propellant feeding. Based on previous test results of PET-100 thrusters, the kept voltage was ±2000 V.

However, the designed propellant feeding rate using the FEP tubing was 10 $\mu$g/s, and it would take approximately 179.7 hours to fill in the roughly 5 ml empty space of the porous material inside the thruster. This slow feeding was observed in the initial tests of this study. Hence, a flow resistance management (FRM) system was built, where a bypass line with a higher flow rate was added to the system to reduce the initial propellant feeding time. The bypass line was a 10 cm long rubber tubing of 1/8 inch outer diameter and 1.651 mm inner diameter, which has a significantly smaller fluidic impedance than the nominal feeding line with a length of 2.1 m and an inner diameter of 0.25 or 0.15 mm. The bypass line was connected in parallel with the nominal flow 1/16 inch FEP tubing via two Union Tee Swagelok connectors, as illustrated in Figure 2 and Figure 5. A solenoid pinch valve was mounted on the bypass line, controlling its flow ON/OFF. The bypass line was only used in the initial feeding stage for the propellant to fill up the porous materials in the thruster. When the electrospray emission was detected, the pinch valves shut off the flow in the byline line, and the delivery system transited to the nominal flow regime of the 1/16 inch FEP tubing.

The feeding system configuration can be segmented into 3 sections: Section 1 is the tubing part connecting the propellant tank to the FRM system , Section 2 is the tubing in the FRM system, and Section 3 is the tubing connecting the FRM system to the thruster. Four different flow resistance configurations were calculated, and the tubing diameters and lengths are shown in Table 1, where $d_1$, $d_2$ and $d_3$ are the inner diameter of the tubing Section 1, Section 2 and Section 3, and $l_1$, $l_2$ and $l_3$ are the length of the tubing Section 1, Section 2 and Section 3, respectively. In the bypass flow configuration, the pinch valve opens the flow through the 10 cm long 1/8 inch tubing in the flow resistance management system; whilst in the nominal flow configuration, the pinch valve closes and propellant is only fed through the 2.1 m

**Table 1 Tubing size specifications of the different flowing configurations used in flow rate calculations.**

| Configuration | $d_1$, mm | $l1$, m | $d_2$, mm | $l2$, m | $d_3$, mm | $l3$, m |
|---|---|---|---|---|---|---|
| Bypass flow | 1.651 | 0.3 | 1.651 | 0.1 | 1.651 | 1.2 |
| Nominal flow | 1.651 | 0.3 | 0.25 | 2.1 | 1.651 | 1.2 |
| ID250 tubing | 0.25 | 2.1 | - | - | - | - |
| ID150 tubing | 0.15 | 2.1 | - | - | - | - |

long 150 $\mu$m inner diameter tubing in the FRM system.

The propellant flow rate and the time required to fill the thruster are calculated and shown in Figure 6. As the propellant filling through the tube, the flow impedance increases and the flow rate decreases. In the nominal feeding configuration, a rapid increase in fluidic impedance occurred at roughly 0.2 to 0.4 s. This is when the fluid fills up the 30 cm long 1.651 mm inner diameter tubing and starts to enter the 2.1 m long 250 $\mu$m inner diameter nominal feeding tube. As the liquid continues to fill in the nominal feeding tube, the fluidic impedance rises closer to that of the configuration using a single tubing of 2,1 m long and 250 $\mu$m. These calculations suggest that using the nominal feeding line would take more than 100 hours to fill in the dry materials in the thruster, whilst this process can be completed in less than 20 minutes using the bypass line.

## V. Test Apparatus

The test and verification of the pressurized propellant-feeding electrospray thruster were conducted in the David Fearn Electric Propulsion Laboratory at the University of Southampton. Two vacuum chambers were used throughout this study, as shown in Figure 7(a), the vacuum chamber A is equipped with a scroll-type roughing pump and a turbopump, which remained $10^{-5}$ to $10^{-6}$ mbar throughout the electrospray thruster operation; and vacuum chamber B is equipped with a oil-sealed roughing pump and a diffusion pump, which was kept at the level of $10^{-5}$ mbar throughout the test.

The power supply used in these electrospray thruster tests was AMT-5B20-L1 Ultra High-Speed High-Voltage Amplifier sourced from Matsusada Precision Inc., with the voltage output limit of ±5 kV and the current limit of ±20 mA. The plume current collector has a molybdenum collecting plate. A nickel grid, MN17 sourced from Precision Eforming Ltd., was placed 5 mm away in front of the collecting plate. Throughout the tests, the grid was applied with -30 V to suppress possible emissions of secondary electrons from high-energy particle collision on the plate. The collector and the thruster were mounted on a set of aluminum profiles. In pressurized electrospray thruster tests, propellant flooding over the emitter was found to be a common issue causing test failures. In order to reduce the risk of gravity-induced propellant overflowing, the thruster was tested vertically, with the electrospray firing upward to the horizontally placed plume current collector, as shown in Figure 7(b).

## VI. Propellant Flow Rate Validation

The propellant flow rate was validated in tests. First, the flow rate using only the feeding tubing was quantified. Then with the thruster was connected, the propellant feeding effectiveness was tested.

### A. Flow Rate of the Tubing

The experimental setup was similar as shown in Figure 2. The propellant was stored in a beaker inside the 6-way cross vacuum chamber, and a 1/8 inch tubing was connected between the 6-way cross and the test chamber. The tubing end inside the 6-way cross was submerged in the propellant liquid, and the tubing end in the test chamber was placed in an empty beaker. The test chamber was then pumped down to a high vacuum while the pressure in the 6-way cross was controlled using solenoid valves and a LabVIEW feedback program. The propellant was allowed to fill in the beaker for 120 minutes in low flow rate cases or 60 minutes in high flow rate cases. The mass of the beaker, including liquid, was measured before and after the test, using a Mettler Toledo mass balance, model WMS404C-L/01. The mass flow rates were then calculated based on mass change over time.

The tests included tubing with diameters of 150 $\mu$m and 250 $\mu$m, and lengths of 1.1 m and 2.1 m. The propellant feeding pressures ranged from 0.2 bar to 1 bar. The measurement results are summarized in Figure 8, where calculated theoretical propellant flow rates are also shown for comparison.

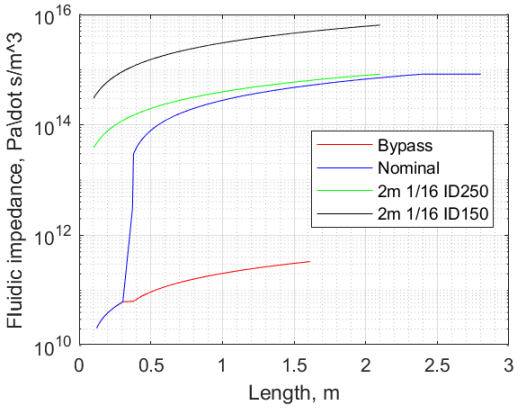


(a) Propellant feeding length in the tubing and the corresponding fluidic impedance.

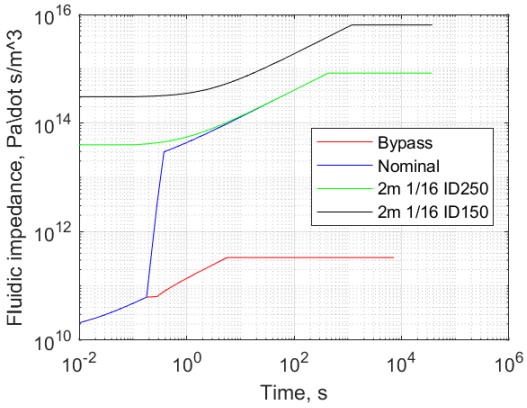


(b) Propellant feeding time in the tubing and the corresponding fluidic impedance.

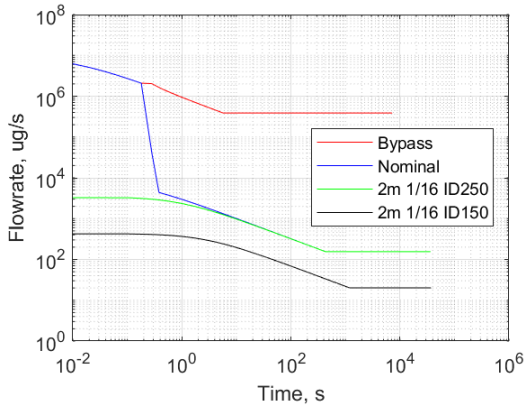


(c) Propellant feeding time and the corresponding mass flow rate.

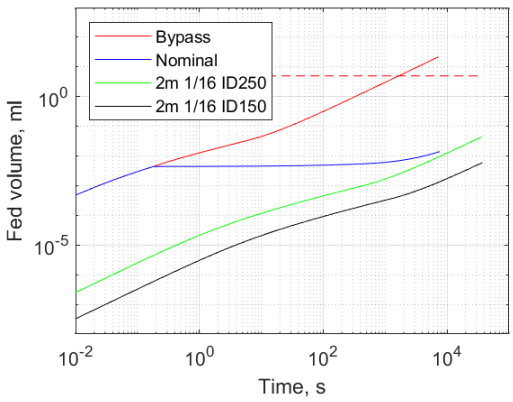


(d) Propellant feeding time and the corresponding filled volume in the thruster, where the dotted red line indicates the volume required to fully fill the space in the thruster.

**Fig. 6 Calculations of the transient propellant flow rate and time needed to fill the thruster using different flow resistance configurations.**

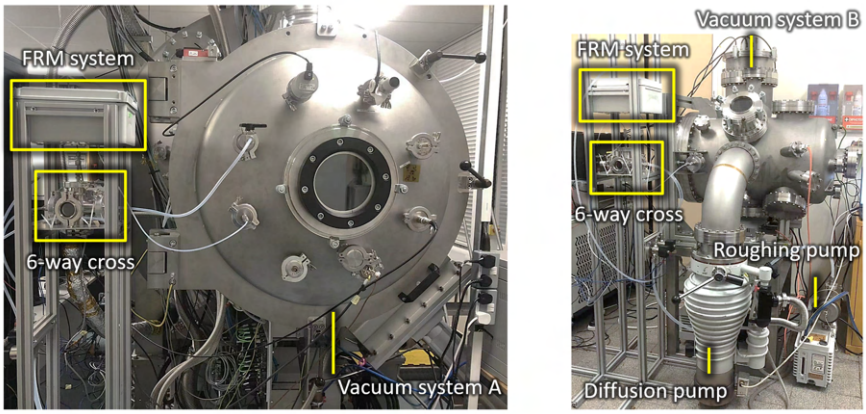


(a) Vacuum chambers.

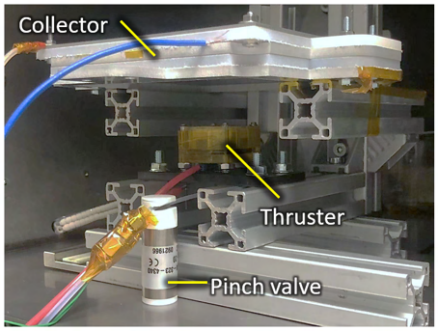


(b) Thruster and collector set up.

**Fig. 7 Vacuum systems used in the pressurized electrospray tests.**

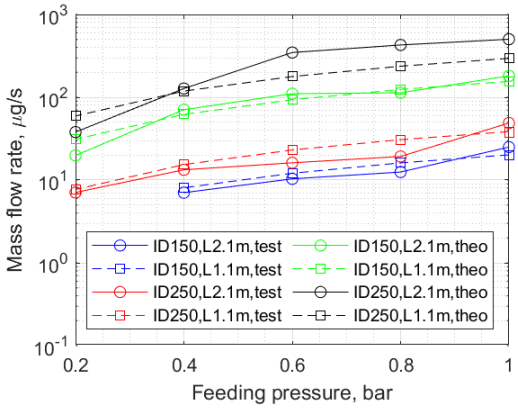


**Fig. 8 The comparison between experimentally validated flow rates and the calculated theoretical values.**

As predicted by theoretical calculations, the tested propellant mass flow rate proportionally decreases with longer tubing lengths, and significantly decreases with smaller tubing diameters. Most of the tested flow rate results are within a 30% error range of the theoretical values, with the exceptional high error ranges in the high flow rate case with the tubing diameter of 250 $\mu$m and the tubing length of 1.1 m.

### B. Considerations with the Thruster Flow Rates

The flow rates measured using these tubing can only be used as guidelines when designing the propellant flow to the thruster, but their values do not represent the actual thruster flow rates. With the thruster connected to the tubing for electrospraying, there are two more considerations: the added fluidic impedance from the porous materials, and the Laplace pressure formed from the curvature liquid surface on the emitter top side.

The additional fluidic impedance induced by the porous materials, $Z_p$, can be worked out using Darcy's law,

$$Z_p = \frac{\Delta P}{Q} = \frac{\mu L_p}{-\kappa A_p}, \tag{2}$$

where $\kappa$ is the permeability of the porous material, $A_p$ is the cross-section area of the porous material relative to the flow direction, and $L_p$ is the length of porous material along the flow direction. The permeability significantly depends on the porosity and material of the porous medium, meaning that the P0 reservoir would have much higher permeability than the P5 emitter. As a partial case of Darcy's law, the Kozeny–Carman equation can be used to estimate the fluidic impedance of a porous material. The Kozeny-Carman equation assumes the porous material is a packed bed of solids, and estimates the permeability

$$\kappa = \Phi_s^2 \frac{\epsilon^3 D_p^2}{150(1-\epsilon^2)^2}, \tag{3}$$

where $\epsilon$ is the porosity of the porous bed, $D_p$ is the average diameter of packed solids, and $\Phi_s$ is the sphericity of the particles in the packed bed, which equals 1 for spherical particles. However, the porous materials used in this study are sintered particles, making it difficult to estimate particles' average diameter $D_p$ and the sphericity $\Phi_s$, and using the Kozeny-Carman equation to estimate the permeability would introduce a significant inaccuracy.

Figure 9 shows an attempt to quantify the fluidic impedance induced by the porous material and compares it with the propellant feeding tubes. The porous material is only based on the dimensions of the emitter substrate without the pyramidal emission tips. The cross-section area is 9 cm$^2$, and the thickness of the substrate is 2 mm. The porous emitters used in electrospray tests are usually P5 and P4 grades, with the pore sizes of 1 to 1.6 $\mu$m and 10 to 16 $\mu$m, respectively. Here the average diameter of the sintered porous particles is assumed to be in a similar range to the pore size. As the sphericity of sintered glass particles is also unidentified, the calculation results consider the sphericity ranging from 0.1 to 1. The porosity of the porous material is assumed to be 0.5. The fluidic impedance of the nominal propellant feeding tubes is also included in the plot, including the maximum impedance using the 2.1 m tubing with 150 $\mu$m inner diameter and the minimum impedance using the 1.1 m tubing with 250 $\mu$m inner diameter. The results suggest that the particle sphericity and average diameter significantly affect the permeability and fluidic impedance. With a smaller particle diameter, the fluidic impedance of the porous materials can be substantially higher than that of the propellant feeding line. Note that the pyramidal porous structures on the emitter were not taken into the calculation, which should further increase the fluidic impedance as the cross-section area is smaller than the substrate.

The accurate value of permeability can be experimentally worked out in a calibration test, where a known pressure is applied and the corresponding flow rate is measured.

Another complication is the spontaneously pressure balancing action of a liquid in a porous material. Depending on the wettability of the liquid on the porous material, the liquid-vacuum boundary form a curvature from surface tension, which, in this case, points outward and creates a negative Laplace pressure. In a porous material, the Laplace pressure, $P_L$, can be expressed as

$$\Delta P_L = \gamma\left(\frac{1}{R_x}\frac{1}{R_y}\right) \approx \gamma\frac{2}{R_p}, \tag{4}$$

where $\gamma$ is liquid surface tension, $R_x$ and $R_y$ are the principle radii of the liquid-vacuum boundary curvature, and $R_p$ is the equivalent radius of the porous cavities.

In a conventional passive-fed electrospray thruster featuring a porous emitter and a porous reservoir, the Laplace pressure on the emitter side is stronger than that on the reservoir side, which pulls the liquid upward to the emitter. This movement lasts until the liquid boundary reaches the top of the emitter surface, where it deforms and resulted

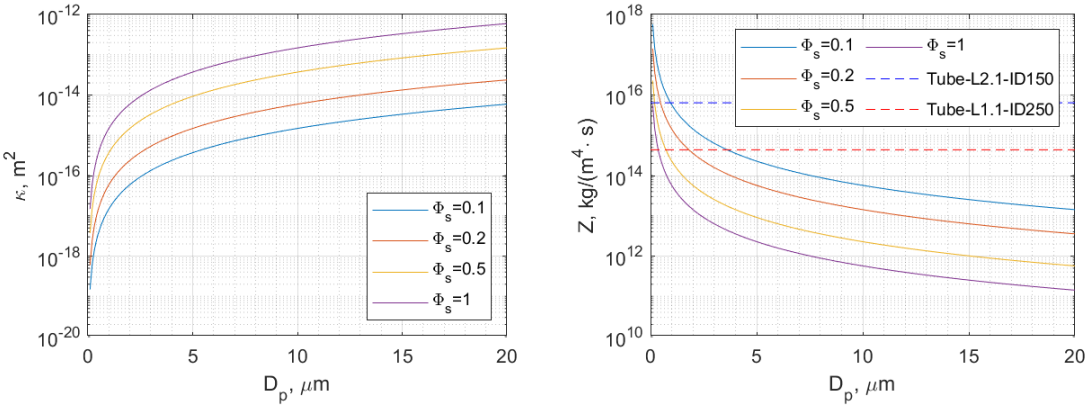


(a) Permeability.

(b) Fluidic impedance.

**Fig. 9 Permeability and fluidic impedance of a porous substrates with different values in particle sphericity and average diameter.**

in a curvature with a Laplace pressure equivalent to that in the reservoir, as illustrated in Figure 10(a) and Figure 10(b). As the thruster was mounted facing upward to reduce the flooding risk, the effect of gravity also contributes to the final static curvature radii on the emitter side. When electrospray emission starts, the extraction of ions creates a new positive pressure on the emission sites, resulting in the liquid being pulled upward to the emitter, sustaining the electrospray emission. Thus, the flow rate of a passive-fed electrospray thruster equals the negative pressure difference from extraction divided by the fluidic impedance, expressed as

$$Q_1 = \frac{P_{ext}}{Z_p} \tag{5}$$

where $P_{ext}$ is the positive pressure created on emitter tips from electrospray emission. The pressure configuration is illustrated in Figure 10(c).

However, the pressure configuration in a pressure-feeding electrospray thruster is different. When only a minor pressure is applied on the propellant, it is possible that the liquid on the emitter side deforms into a curvature with a negative pressure (against the flow direction) pushing the propellant and reaching a static state, as illustrated in Figure 10(d). When electrospray emission starts, the flow rate would be higher than that of the passive-fed thruster (assuming that the fluidic impedance is the same) due to the additional driving pressure applied on the propellant, expressed as

$$Q_2 = \frac{P_{ext} + P_{prop}}{Z_p + Z_t}, \tag{6}$$

where $P_{prop}$ is the pressure applied to the propellant, $Z_t$ is the fluidic impedance of the propellant feeding tubing. The pressure configuration of the thruster during electrospray emission with pressure-feeding is illustrated in Figure 10(f).

If the pressure applied on the propellant is relatively high, the negative Laplace pressure on the emitter side will not be able to maintain the static state of the liquid, which then results in propellant overflowing and flooding, as illustrated in Figure 10(e), and electrospray emission will fail to start. As a hypothesis, assuming that the electrospray emission was already started at low or no propellant feeding pressures, it is possible that increasing the propellant feeding pressure may not flood the thruster, but instead, it could sustain the electrospray emission at a higher flow rate.

More work needs to be done to quantify the pressure induced by electrospray emission. It is likely that the flow rate and the extraction pressure are correlated. Thus, in this study, the propellant flow rate in electrospray emission was only characterized based on test results.

### C. Feeding the Thruster

In order to measure the actual flow rate, the vacuum end of the feeding tubing was connected to a PET-100 thruster. At times, gas bubbles are entrained in the tubing during the propellant feeding. The movements of these bubbles were

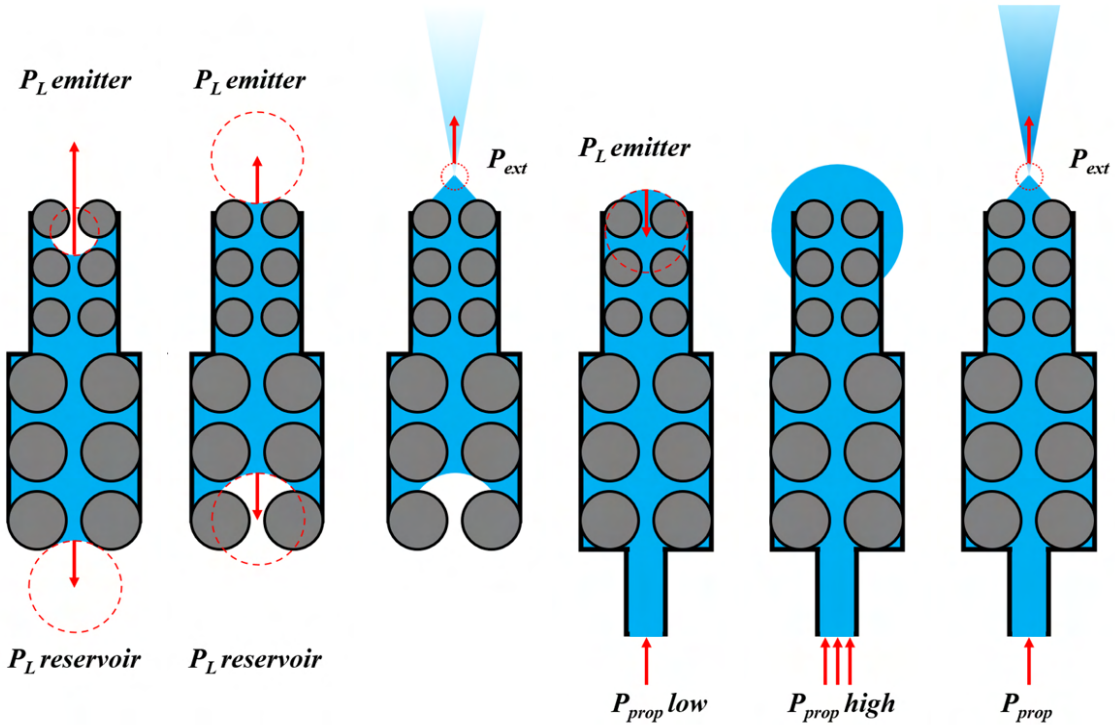


(a) Passive initial. (b) Passive settled. (c) Passive emission. (d) Pressure settled. (e) Pressure overflow. (f) Pressure emission.

**Fig. 10 Schematics of the pressure configuration before and during porous-emitter electrospray emission in a passive-feeding regime and in a pressure-feeding regime. The porous material microstructures are simplified to a packed bed of particles only for the illustration of the concept.**

**Table 2 Propellant flow rate calculated from tracking gas bubble movement.**

| $t_0, min$ | $\Delta t, min$ | $\Delta l, mm$ | $\frac{\Delta l}{\Delta t}, mm/min$ | $\Delta V/\Delta t, mm^3/s$ | $\Delta M/\Delta t, \mu g/s$ |
|---|---|---|---|---|---|
| 0 | 4 | 15.5 | 3.875 | 0.138 | 178.91 |
| 4 | 3 | 8.1 | 2.700 | 0.096 | 124.66 |
| 7 | 9 | 23.2 | 2.578 | 0.092 | 119.02 |
| 16 | 6 | 11.5 | 1.917 | 0.068 | 88.49 |
| 22 | 4 | 4.1 | 1.025 | 0.037 | 47.33 |
| 26 | 9 | 15.9 | 1.767 | 0.063 | 81.57 |
| 35 | 13 | 12.3 | 0.946 | 0.034 | 43.68 |
| 48 | 8 | 14.2 | 1.775 | 0.063 | 81.95 |

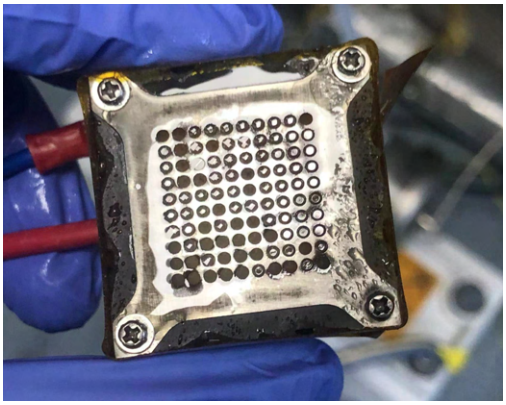

**Fig. 11 Propellant flooding on the top side of the thruster.**

used to calculate the propellant flow rate. The tubing used for gas bubble tracking was a 1/8 inch PFA tubing sourced from Swagelok, with an inner diameter of 1.651 mm. This 1/8 inch PFA tubing was a segment connected downstream of the FRM system. With the FRM system using a 2.1 m long 1/16 inch 250 $\mu$m inner diameter tubing, in the initial propellant filling stage, the gas bubble movement was recorded, and the flow rates are calculated, as summarized in Table 2. The $t_0$ is the starting time of the measurement, $\Delta t$ is the time of each measurement, $\Delta l$ is the movement length of the gas bubble in the tubing, and $\Delta V/\Delta t$ and $\Delta M/\Delta t$ are the volumetric flow rate and the mass flow rate of the propellant. The propellant feeding pressure was 1 bar in this test. Note that this test was in the stage of filling the dry porous materials in the thruster, when the propellant filling the tubing was already completed.

The theoretical flow rate in this flow configuration after filling the tubing is 155.48 $\mu$g/s, as shown in Figure 6(c). At the beginning of this test, the measured mass flow rate from gas bubble tracking was approximately 178.91 $\mu$g/s, close to the theoretical value. The measured flow rate gradually decreases with time. From 48 mins to 56 mins, the mass flow rate was 81.95 $\mu$g/s, only 45.8% of the initial flow rate. The reason for the decreased flow rate, as discussed in Section VI.B, is likely due to the increasing fluidic impedance of porous materials as the propellant progresses. A similar test was done using a 2.1 m long and 150 $\mu$m inner diameter tubing placed in the FRM system, and the measured flow rate changed from 7.18 $\mu$g/s to 6.51 $\mu$g/s in an 84 mins test with the theoretical flow rate of 20.15 $\mu$g/s.

As predicted, the gas bubble tracking tests suggested that the propellant flow rate was low. It would take 10 to 100 hours to fill the dry porous materials in the thruster, justifying the necessity of the bypass propellant feeding line with high flow rates. The bypass line was then tested using the same feeding pressure, and the propellant delivery proved to be highly effective. The feeding rate was much higher than using the 1/16 inch tubing, to the level that the gas bubble tracking method cannot be used. However, the significantly increased flow rate also induced risks of propellant overflowing the emitter and flooding the topside of the thruster, with an example shown in Figure 11.

In order to reduce the propellant flooding risk, a feedback control program was implemented. A voltage was kept between the emitter and the extractor. Once an emission current is detected, it triggers the shut-off of propellant delivery valves and changes the 6-way cross chamber pressure to vacuum. The ionic liquid propellant is incompressible, but gas bubbles possibly entrained or outgassed in the feeding line are compressible, possibly creating a lingering pressure and

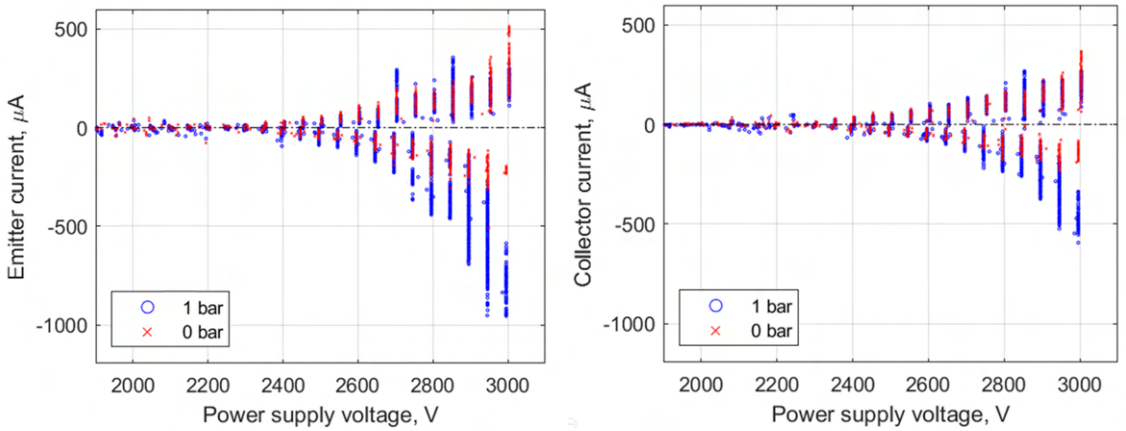


(a) Emitter current-voltage plots.

(b) Collector current-voltage plots.

**Fig. 12 Current-voltage plots at feeding pressures of 0 bar and 1 bar using collected raw data.**

causing a delayed effect in propellant feeding. In order to avoid this delayed effect from resulting in propellant flooding during the bypass line filling stage, the valves were turned on for 10 s and then turned off for 30 s to allow the lasting pressure to settle the progression of liquid. This ON-OFF valve sequence was repeated until the electrospray emission current was detected.

## VII. Preliminary Electrospray Test Results

With the thruster filled with propellant from the pressure delivery system, preliminary electrospray tests were conducted at different propellant feeding pressures. The thruster was first tested with 1 bar of pressure in the 6-way cross chamber, which gradually decreased to near 0 bar. The current-voltage characteristics of the thruster were measured, with example raw data collected at 0 bar and 1 bar shown in Figure 12.

The power supply voltage was gradually increased from 2000 V to 3000 V, with steps of ±50 V. At each measured voltage, the measured current values experienced some variations, indicating the levels of current instability. These current variations are displayed as the vertical data lines in the current-voltage plots. Figure 12(a) shows the emitter current monitored using the power supply, and Figure 12(b) shows the current received on the current collector. Both current-voltage plots have similar near-exponentially growing trends. The negative current had higher magnitudes than the positive current at the same voltage levels. In the positive polarity operation, the emitter current and the collector current had similar values up to +2650 V, after which the collector current was noticeably smaller than the emitter current. In the negative polarity operation, the threshold where the collector current started to show markedly lower values than the emitter current was -2500 V. The differences between the emitter current and the collector current have been widely observed in different electrospray tests, one of the main reasons was believed to be that the plume increased with voltage to a point that a significant amount of plume current was geometrically intercepted by the extractor electrode. Another possible reason is that plume profile had a wide angle that the collector plate could not collect the whole plume. However, this is unlikely to be the dominant reason for the discrepancy between the emitter current and the collector current. As in these tests, the collector was placed rather close to the thruster, with an interceptable half plume angle of approximately 70°. Therefore, the collector should be able to capture the majority of the plume particles, given that this type of electrospray thruster usually has a plume spreading from 50 to 60°.

The current-voltage characteristics between 1 bar and 0 bar of propellant feeding pressure are noticeably different. In order to illustrate the discrepancies more explicitly, the featuring data in the raw data plots were extracted and shown in Figure 13(a), which also includes the current-voltage plots at 0.4 bar and 0.8 bar. It is clear that the propellant feeding pressure has marked effects on the performance of a porous-emitter electrospray thruster. With the pressure changing from 1 bar to 0 bar, the positive side of the emitter current only had minor variations, whilst the negative emitter current experienced significant decreases. The emitter current at ±3000 V at different propellant feeding pressures are summarized in Figure 13(b).

As the propellant flow rate supposedly increases with higher feeding pressure, the emission current was expected

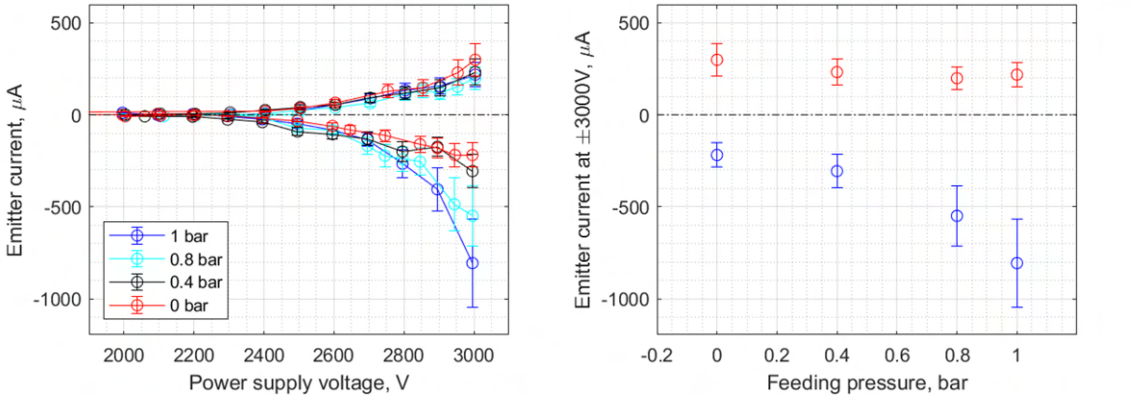


(a) Summarized emitter current-voltage plots at 0, 0.4, 0.8 and 1 bar of feeding pressure.

(b) Emitter current at different propellant feeding pressures with the power supply voltage of ±3000 V.

**Fig. 13 Summarized emitter current variation at different voltages and different propellant feeding pressures.**

to increase, which only occurred in the negative side. It is possible that the propellant feeding pressure increase only enhances the emission rates of anions, but only has limited or no effect on the emission of cations. However, it should be noted that these are current-voltage measurements, which only confirms the change of charges of the emission. A hypothesis is that in the negative polarity, more anions were extracted from the emitter as the propellant feeding pressure increase. Whilst in the positive polarity, the number of cations extracted didn't change much with the pressure, but at the same time the cations might be entrained in heavy neutral droplets when extracted from the emission sites. The neutral droplets contributes to a higher flow rate but does not affect the measured current. A time-of-flight characterization is required to confirm the mass of the emitted particles, which will be completed in future work.

The plume current collector was inspected after the pressurized propellant feeding test, as shown in Figure 14. Newly formed patterns were found on the plate directly aligned with the thruster firing position. The shape of the pattern roughly fits in a square outline with several sections missing. The emission area of the thruster is squared, but its emission current density was not uniform across the emission tips array due to misalignment errors between the emitter and the extractor. The asymmetrical spatial features of the plume profile were characterized in a related study using the same thruster design [11]. The original molybdenum plate was entirely dark grey colored before the test, whilst the new patterns had a brighter silver-colored background with dark brown speckles mixed within the entire bright area. This is likely evidence of accumulated collision of droplets and ions. In tests, high-energy ions emitted from EMI-$BF_4$ were found to be effective in polishing molybdenum material to reflective surfaces. As the tiny brown speckles only appeared within the ion-impinged area, they are likely imprints of droplets that impact the surface. Note that these brown speckles were not found in previous tests of PET-100 thrusters that used passive feeding methods and demonstrated purely ionic emission. These results suggest that changing the propellant delivery pressure resulted in the electrospray changing emission modes among ionic emission, droplets emission, and ion-droplet mixed emission, directly affecting the thrust and specific impulse. These imprints were accumulated results with the pressure varied from 1 bar to 0 bar, making it impossible to identify the differences among different pressures. This finding suggests a method to analyze the droplet emission. With the thruster operating at a set condition of pressure and voltage, the statistical distribution regarding the size and locale of the speckle imprints will be analyzed in future work. The particle imprints analysis will be combined with time-of-flight measurements to provide valuable information on the plume particle composition, thrust, and specific impulse.

## VIII. Conclusion

The aim of this study is to investigate the effects of the propellant feeding pressure on the performance the electrospray thruster.

A pressurized propellant feeding system for porous-emitter electrospray thruster was developed. The relationships among propellant flow rate, feeding pressure, tubing diameter, and tubing length were calculated. The results suggest that the flow rate proportionally increases with the feeding pressure, inverse-proportionally decreases with the tubing

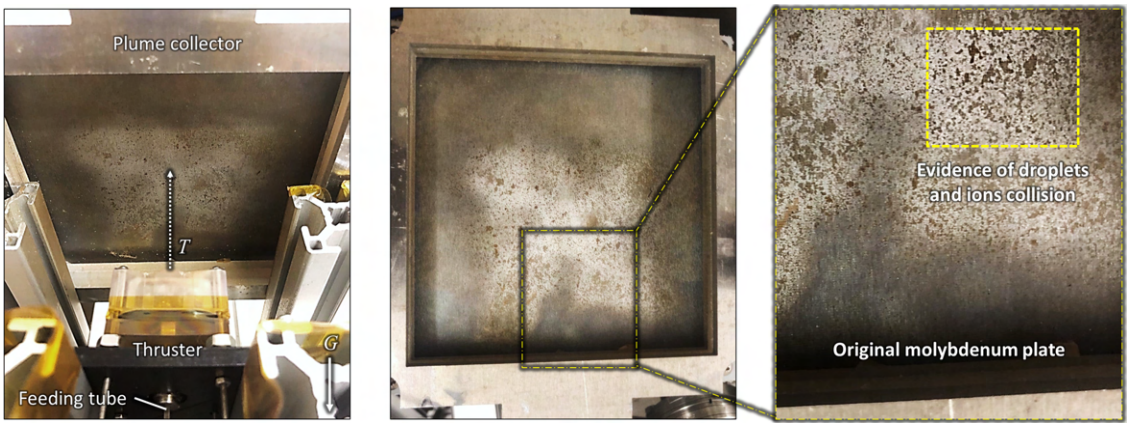


**Fig. 14 Post-test inspection of the plume current collector plate.**

length, and drastically decreases with smaller tubing diameters, as was confirmed with experimental calibration tests. Tubing with inner diameters of 150 $\mu$m and 250 $\mu$m and lengths of 1.1 m and 2.1 m were calculated and experimentally tested. The lowest flow rate found in tests was 7.04 $\mu$g/s using 2.1 m long tubing with the inner diameter of 150 $\mu$m at 0.4 bar of feeding pressure, and the highest flow rate was 502.49 $\mu$g/s using 1.1 m long tubing with the inner diameter of 250 $\mu$m at 1 bar of feeding pressure. Most of the tested flow rates were close to the theoretical values, within the error range from ±7% to ±30%, with the error increasing at higher flow rates. In order to avoid false characterization in the passive-feeding mode and ensure that the propellant feeding pressure was indeed in action, the thruster was fed from a dry state without pre-filling the porous materials. The propellant flow rate using nominal flow lines were tested using gas bubble tracking method, the flow rate ranged from 178.91$\mu$g/s to 81.95$\mu$g/s using the 250$\mu$m ID tubing and 7.18$\mu$g/s to 6.51$\mu$g/s using 150 $\mu$m ID tubing. As it would take more than one hundred hours to fill the thruster empty space using the nominal flow rate, a bypass line with significantly higher flow rate was designed in the flow resistance management system, which effectively reduced the propellant filling time to 10 to 20 minutes.

The theoretical flow rate faces two complications when a porous-emitter electrospray thruster is connected to the end of the feeding tube. The porous materials in the thruster added additional fluidic impedance to the propellant feeding system, but the thin unsealed gaps between the porous material and the thruster casing bring uncertainty to the effective value of the additional fluidic resistance. During electrospray emission, the pressure induced by ions/droplets leaving the liquid also contributes to the final flow rate. The extraction-induced pressure was not characterized in this study. Therefore, the propellant flow rates with the thruster connected were measured only in tests based on gas bubbles' movement in the propellant feeding tube.

The current-voltage characteristics of the electrospray thruster at different propellant feeding pressures were measured. Overall, the thruster demonstrated relatively high emitter current, with maximum value of approximately +216.52 $\mu$A at +3000 V and -807.54 $\mu$A at -3000 V, tested at 1 bar of propellant feeding pressure. In comparison, the current values at 0 bar of propellant feeding pressure were +300.29 $\mu$A at +3000 V and -217.18 $\mu$A at -3000 V. The thruster emitted more substantial negative currents at higher propellant feeding pressures, whilst the emitted current at positive voltages only had minor changes at different feeding pressures.

This preliminary study demonstrated that it is feasible to use a pressurized propellant feeding system on an electrospray thruster, and the propellant feeding pressure can cause marked changes to the thruster performance. Further investigations are encouraged, including reducing gas bubbles in the propellant feeding line, measuring the effective flow rate, and using a time-of-flight system to characterize the masses of plume particles.

## Acknowledgments

The research reported here was partially supported by the Defense Advanced Research Projects Agency Grant No.: HR00112110003. The content of this paper does not necessarily reflect the position or the policy of the Government, and no official endorsement should be inferred. We thank the Engineering Design and Manufacturing Centre (EDMC) at the University of Southampton for manufacturing our testing equipment.

## Data Availability

The data that support the findings of this study are available from the corresponding author upon reasonable request.

## References


[1] Dale, E., Jorns, B., and Gallimore, A., "Future directions for electric propulsion research," *Aerospace*, Vol. 7, No. 9, 2020, pp. 1–30.

[2] Courtney, D. G., and Shea, H., "Influences of Porous Reservoir Laplace Pressure on Emissions From Passively Fed Ionic Liquid Electrospray Sources," *Applied Physics Letters*, Vol. 107, No. 10, 2015, pp. 1–5.

[3] Krejci, D., Mier-Hicks, F., Thomas, R., Haag, T., and Lozano, P., "Emission Characteristics of Passively Fed Electrospray Microthrusters with Propellant Reservoirs," *Journal of Spacecraft and Rockets*, Vol. 54, No. 2, 2017, pp. 447–458.

[4] Courtney, D. G., Alvarez, N., and Demmons, N. R., "Electrospray Thrusters for Small Spacecraft Control: Pulsed and Steady State Operation," *2018 Joint Propulsion Conference*, American Institute of Aeronautics and Astronautics, 2018, pp. 1–15.

[5] Natisin, M. R., and Zamora, H. L., "Performance of a Fully Conventionally Machined Liquid-Ion Electrospray Thruster Operated in PIR," *International Electric Propulsion Conference 2019*, 2019, pp. 1–16.

[6] Ma, C., Bull, T., and Ryan, C. N., "Plume Composition Measurements of a High-Emission-Density Electrospray Thruster," *Journal of Propulsion and Power*, Vol. 37, No. 6, 2021, pp. 816–831.

[7] Rovey, J. L., Lyne, C. T., Mundahl, A. J., Rasmont, N., Glascock, M. S., Wainwright, M. J., and Berg, S. P., "Review of multimode space propulsion," *Progress in Aerospace Sciences*, Vol. 118, 2020, p. 100627.

[8] Lyne, C. T., Rovey, J., and Berg, S. P., "Monopropellant-Electrospray Multimode Thruster Testing Results: Electrospray Mode," *AIAA Propulsion and Energy 2021 Forum*, AIAA Propulsion and Energy Forum, American Institute of Aeronautics and Astronautics, 2021.

[9] Bruno, A., Schroeder, M., and Lozano, P. C., "Characterization of Electrospray Thrusters with HAN-Based Monopropellants for Multimode Propulsion Applications," *AIAA SCITECH 2022 Forum*, AIAA SciTech Forum, American Institute of Aeronautics and Astronautics, 2021.

[10] Berg, S. P., Rovey, J., Prince, B., Miller, S., and Bemish, R., "Electrospray of an Energetic Ionic Liquid Monopropellant for Multi-Mode Micropropulsion Applications," *51st AIAA/SAE/ASEE Joint Propulsion Conference*, AIAA Propulsion and Energy Forum, American Institute of Aeronautics and Astronautics, 2015.

[11] Ma, C., Messina, V., Ryan, C. N., Rovey, J. L., Putnam, Z., Lembeck, M., and Berg, S., "Plume Study of an Electrospray Thruster Using a HAN-Based Dual-Mode Ionic Liquid Propellant," *Proceedings of the 37th International Electric Propulsion Conference*, Electric Rocket Propulsion Society, Cambridge, MA, 2022.

[12] Ma, C., and Ryan, C., "Plume Characterization of a Porous Electrospray Thruster," *Proceedings of the 36th International Electric Propulsion Conference*, 2019, pp. 1–19.

[13] Ziemer, J., Marrese-reading, C., Dunn, C., Romero-wolf, A., Cutler, C., Javidnia, S., Le, T., Li, I., Franklin, G., and Barela, P., "Colloid Microthruster Flight Performance Results from Space Technology 7 Disturbance Reduction System," *Proceedings of the 35th International Electric Propulsion Conference*, Electric Rocket Propulsion Society. Also IEPC-2017-578, Atlanta, Georgia, 2017, pp. 1–17.

[14] Krpoun, R., "Micromachined Electrospray Thrusters for Spacecraft Propulsion," Ph.D. thesis, Ecole Polytechnique Federale De Lausanne, 2009.

[15] Ryan, C., Daykin-Iliopoulos, A., Stark, J. P. W., Salaverri, A. Z., Vargas, E., Rangsten, P., Timmerman, J., de Jong, M., Visee, R., Vliet, L. V., Sanders, B., Straathof, M., Nardini, F. T., Pul-verboom, V. V., Dandavino, S., Chakraborty, S., Courtney, D. G., Belloni, F., Richard, M., and Shea, H. R., "The MicroThrust MEMS electrospray thruster : results and conclusions," *AAAF-ESA-CNES Space Propulsion 2014*, Cologne, Germany, 2014, pp. 1–10.

[16] Alexander, M. S., Stark, J., Smith, K. L., Stevens, B., and Kent, B., "Electrospray Performance of Microfabricated Colloid Thruster Arrays," *JOURNAL OF PROPULSION AND POWER*, Vol. 22, No. 3, 2006, pp. 620–627.

[17] Demmons, N., Alvarez, N., Wood, Z., Strain, M., Company, B., and Ziemer, J., "Colloid Micro-Thruster (CMT) Component Development & Testing Towards Meeting LISA Mission Requirements," *Proceedings of the 36th International Electric Propulsion Conference*, Electric Rocket Propulsion Society, Vienna, Austria, 2019, pp. 1–22.

[18] Bruno, A. R., and Lozano, P. C., "Design and Testing of a Propellant Management System for Bimodal Chemical-Electrospray Propulsion," *IEEE Aerospace Conference Proceedings*, Vol. 2021-March, IEEE Computer Society, 2021.

[19] Ma, C., "Design and Characterisation of Electrospray Thrusters with High Emission Density," Ph.D. thesis, University of Southampton, 2020.

[20] Ma, C., and Ryan, C., "Plume Particle Energy Analysis of an Ionic Liquid Electrospray Ion Source with High Emission Density," *Journal of Applied Physics*, Vol. 129, No. 083302, 2021, pp. 1–11.